Frascati Physics Series Vol. nnn (2001), pp. 000-000
Heavy Quarks at Fixed Target - Rio de Janeiro, Oct. 9-19, 2000

NEW RESULTS ON RARE AND FORBIDDEN SEMILEPTONIC K^+ DECAYS

Peter Truöl
Physik-Institut, Universität Zürich, CH 8057 Zürich, Switzerland

ABSTRACT

Experiment E865 [1)] at the Brookhaven AGS was set up primarily to search for the lepton flavour violating decay $K^+ \to \pi^+\mu^+e^-$ ($K_{\pi\mu e}$) with high sensitivity. The flexibility of the apparatus allowed also to obtain more than an order of magnitude larger than previously available event samples on the following decay modes: $\pi^+e^+e^-$ ($K_{\pi ee}$), $\pi^+\mu^+\mu^-$ ($K_{\pi\mu\mu}$), $\pi^+\pi^-e^+\nu_e$ (K_{e4}), $\mu^+e^+e^-\nu_\mu$, and $e^+e^+e^-\nu_e$. The report focusses on the $K_{\pi\mu e}$ results and those on other lepton flavour violating decays as well as the K_{e4} data, from which a new, quite precise value for the s-wave $\pi\pi$ scattering length can be deduced.

1 The E865 experiment: goals and techniques

The search for a violation of the apparent, but theoretically not well founded lepton number conservation law continues at several laboratories around the

world. Improving the sensitivity beyond existing limits for the decays $\mu^+ \to e^+\gamma$ ($< 1.2\times10^{-11}$) [2] and $\mu^- A \to e^- A'$ ($< 1.7\times10^{-12}$) [3] is the goal of ongoing or planned experiments at the Paul Scherrer Institut (PSI) and Brookhaven National Laboratory (BNL) [4]. The observed evidence for neutrino oscillations [5] has further stimulated the interest in this area. Since extensions of the Standard Model like supersymmetry, leptoquarks, technicolor and other horizontal gauge boson models have been proposed which allow the possibility of flavour changing neutral currents and lepton family violating interactions, the forbidden K decays $K_L^0 \to \mu^\pm e^\mp$ ($< 4.7 \times 10^{-12}$) [6] and $K^+ \to \pi^+\mu^+e^-$ ($K_{\pi\mu e} < 2.0 \times 10^{-10}$) [7] were also investigated. E865 was set up to search for the latter decay with improved sensitivity.

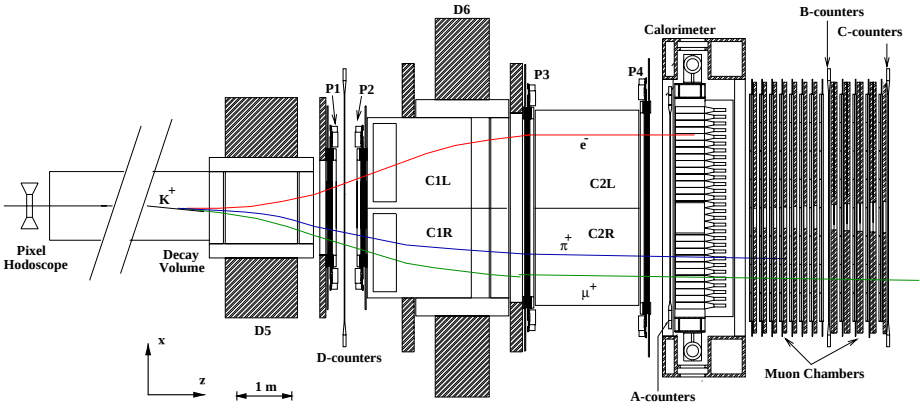

Figure 1: *Plan view of the E865 spectrometer.*

The E865 detector (see Fig. 1) resided in an unseparated 6 GeV/c beam of 1.5×10^7 K^+ accompanied by about 3×10^8 π^+ and p per AGS cycle. About 8% of the K^+ decayed in the 5 m long decay volume. The decay products were separated by charge by a first dipole magnet and then momentum analysed by a second dipole magnet sandwiched between two pairs of proportional chambers. The wire chambers with four planes each were kept at lower voltage in the region were the beam passes. This arrangement yields a resolution of $\sigma_p/p^2 \approx 0.003$, where the momentum p of the decay products ($\pi^\pm, \mu^\pm$ or $e^\pm$) ranges between 0.6 and 3.5 GeV/c. Four gas filled Čerenkov counters were positioned inside and after the spectrometer magnet for $e^\pm$ identification. An electromagnetic

calorimeter of Shashlyk type [8] further helped to separate $e^{\pm}$ from other decay products. It consists of 600 modules, each 15 radiation lengths deep in beam direction. It is followed by an array of 12 planes of proportional tubes separated by iron plates used to discriminate pions against muons.

The event trigger is based on the information from four scintillator hodoscopes, D and A before and after the spectrometer, B and C in front and in the middle of the muon stack. In the lowest trigger level three charged particles are required, each identified by a cluster in the calorimeter and a signal from the A-counter in front of it. Depending on the final state the particle identification signals and topological information is added at higher levels, e.g. a $K_{\pi\mu e}$ candidate is given by an e^- (Čerenkov on beam left filled with H_2 at atmospheric pressure) and two particles on the beam right, one traversing the muon stack, vetoed with signals from the CH_4 filled Čerenkov on beam right. The flexibility of the trigger and particle identification system allowed to accumulate high statistics data samples either concurrently with $K_{\pi\mu e}$ high intensity running or in dedicated runs at lower intensity on the decays $\pi^+e^+e^-$ ($K_{\pi ee}$), $\pi^+\mu^+\mu^-$ ($K_{\pi\mu\mu}$), $\pi^+\pi^-e^+\nu_e$ (K_{e4}), $\mu^+e^+e^-\nu_\mu$, $e^+e^+e^-\nu_e$ for physics analysis and on $\pi^+\pi^0$ ($e^+e^-\gamma$) (K_{Dalitz}) and $\pi^+\pi^+\pi^-$ (K_τ) for normalisation.

The report focusses on the $K_{\pi\mu e}$ results and those on other lepton flavour violating decays as well as the K_{e4} data, from which a new, quite precise value for the s-wave $\pi\pi$ scattering length can be deduced. This quantity plays a central role in the low energy effective theory of strong interactions - chiral perturbation theory (ChPT) [9, 10]. Both the flavour changing neutral current decays $K_{\pi\mu\mu}$ and $K_{\pi ee}$, which will not be discussed here in detail, are known to be dominated in the Standard Model by long-distance effects involving one-photon exchange, and are of interest for ChPT tests, too. Our published results [11, 12] for these decays include precise branching ratios and form factor information, establish firmly the vector nature of the interaction, resolve the discrepancy of older data with $e\mu$ universality, and provide evidence for the existence of a pion loop term calculated in next-to-leading order ChPT.

2 Lepton flavour number violating decays

Not all our $K_{\pi\mu e}$ data have been analysed yet. The data taken during the last running period in 1998 are projected to push the sensitivity limit below the 10^{-11} branching ratio level. Table 1 lists the limits deduced from the 1995 [13]

Table 1: *Upper limits for lepton flavour number violating decays established by experiment E865* [14, 17]*: LFNV: violation of lepton flavour number conservation (L_μ, L_e); LNV: violation of total lepton number conservation ($L = L_\mu + L_e$); G_i: number of quarks and leptons of generation i* [15]*; GV: violation of generation number conservation. (PDG: particle data group* [18]*)*

K^+ decay mode	Branching ratio	Data	Remarks LFNV
$\pi^+\mu^+e^-$	$< 3.9 \cdot 10^{-11}$	$K_{\pi\mu e}$ (1996)	$\Delta L = 0$
$K_{\pi\mu e}$	$< 2.1 \cdot 10^{-10}$	$K_{\pi\mu e}$ (1995)	$\Delta L_e = -\Delta L_\mu = 1$
	$< 2.0 \cdot 10^{-10}$	[Lee 1990]	$\Delta G_1 = \Delta G_2 = 0$
	$< 2.8 \cdot 10^{-11}$	Combined	
	$< 1.0 \cdot 10^{-11}$	Expected (1998)	
$\pi^+e^+\mu^-$	$< 7.0 \cdot 10^{-9}$	PDG	GV, $\Delta L = 0$
$K_{\pi e\mu}$	$< 5.1 \cdot 10^{-10}$	K_{e4} (1997)	$\Delta L_\mu = -\Delta L_e = 1$
			$\Delta G_2 = -\Delta G_1 = 2$
$\pi^-\mu^+e^+$	$< 7.0 \cdot 10^{-9}$	PDG	LNV, GV, $\Delta L = -2$
$K_{\mu e\pi}$	$< 4.9 \cdot 10^{-10}$	K_{e4} (1997)	$\Delta L_\mu = \Delta L_e = -1$
			$\Delta G_2 = 0,\ -\Delta G_1 = 2$
$\pi^-e^+e^+$	$< 1.0 \cdot 10^{-8}$	PDG	LNV, GV
$K_{ee\pi}$	$< 6.3 \cdot 10^{-10}$	K_{e4} (1997)	$\Delta L = \Delta L_e = -2$
			$\Delta G_2 = 1,\ -\Delta G_1 = 3$
$\pi^-\mu^+\mu^+$	$< 1.5 \cdot 10^{-4}$	PDG	LNV, GV
$K_{\mu\mu\pi}$	$< 3.0 \cdot 10^{-9}$	$K_{\pi\mu\mu}$ (1997)	$\Delta L = \Delta L_\mu = -2$
			$\Delta G_2 = \Delta G_1 = -1$

and 1996 data [14]. Figure 2 shows the mass distribution of the few $K_{\pi\mu e}$ candidates remaining after a likelihood analysis. No event is found with a likelihood for the $K_{\pi\mu e}$ hypothesis exceeding 20%. Background events may come from K^+ decays with errors in kinematic reconstruction or particle identification measurements or from accidental combinations of three tracks (dominant contribution). The probabilities to misidentify a π^- as an e^-, or an a π^+ as an e^+ (μ^+) are 2.6×10^{-6} and 1.7×10^{-5} (0.049), while the identification efficiencies for π^+, μ^+ and e^- are 78%, 74% and 55%, respectively. The likelihood distributions constructed for these background events let us then expect 2.6 events below the 20% line indicated in Fig. 2 consistent with the threeevents observed. Combined with earlier data [7] our results yield an upper limit for

the $K_{\pi\mu e}$ branching ratio of 2.8×10^{-11} (see Table 1).

In models described by a horizontal gauge interaction [15, 16] one may use this branching ratio to deduce a limit for the mass of an intermediate boson X by comparison to the allowed decay $K^+ \to \pi^0 \mu^+ \nu_\mu$ ($K_{\mu 3}$):

$$\frac{B.R.(K_{\pi\mu e})}{B.R.(K_{\mu 3})} \approx \frac{16}{\sin^2\theta_c} \left(\frac{g_X}{g}\right)^4 \left(\frac{M_W}{M_X}\right)^4 \Rightarrow (g/g_X) M_X < 60 \text{ TeV}/c^2 \ .$$

Here θ_c is the Cabbibo angle, and g_X and g are the couplings for the new and the weak interaction, respectively.

Unlike $K_{\pi\mu e}$, which only violates lepton flavour conservation, the other decays for which Table 1 lists upper limits, also violate generation number conservation [15]. We used our $K_{\pi\mu\mu}$ and K_{e4} data samples to search for these decays. These data sets were taken with dedicated triggers at lower beam intensity. The $K_{\mu\mu\pi}$ and $K_{e\mu\pi}$ mass plots are shown in Fig. 2 as examples. The most significant reduction of the existing limit [18] (by a factor of 50000) was obtained for $K_{\mu\mu\pi}$, a decay which is sensitive to the same exotic mechanism, which may permit nuclear double β-decay [19].

3 K_{e4} and the $\pi\pi$ scattering length

Since more than 30 years, the K_{e4} decay has been used to study $\pi\pi$-scattering at low energies. The most recent experiment performed by a Geneva-Saclay collaboration at CERN [20] accumulated 30000 events. Using these data and some peripheral $\pi N \to \pi\pi N$ data did lead to the presently generally accepted value for the isoscalar s-wave scattering length of $a_0^0 = (0.26 \pm 0.05)$ (in units of M_π^{-1}).

On the theoretical side $\pi\pi$ scattering is the *golden reaction* for chiral perturbation theory (ChPT) [22]. This low-energy effective theory for the strong interaction makes firm predictions for the scattering length. The pioneering tree level calculation by Weinberg [21] yielded $a_0^0 = 0.156$ ($a_0^2 = -0.046$). The one-loop ($a_0^0 = 0.201$, $a_0^2 = -0.042$ [9]) and the recently completed two loop calculation ($a_0^0 = 0.217$, $a_0^2 = -0.041$ [23, 24]) show a satisfactory convergence. The most recent calculation [10] matches the known chiral perturbation theory representation of the $\pi\pi$ scattering amplitude to two loops with a phenomenological description that relies on the Roy equations (see below). The corrections to Weinberg's low energy theorems for the s-wave scattering lengths are worked

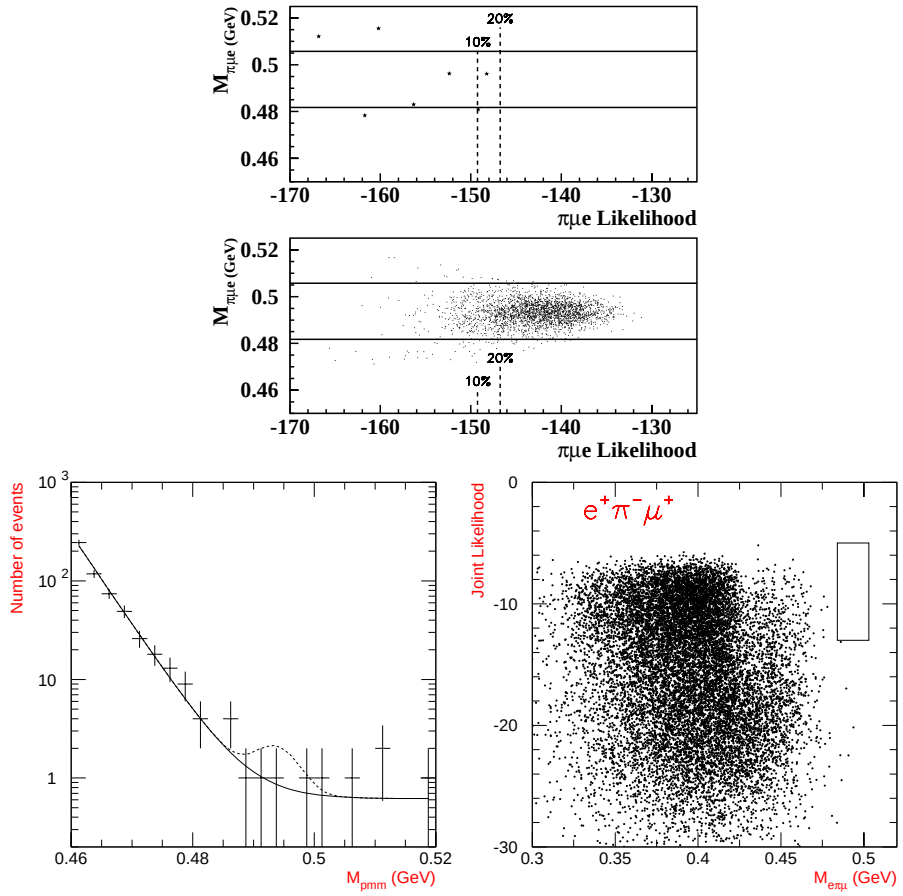

Figure 2: *Top: scatter plot of log-likelihood versus invariant mass for $K_{\pi\mu e}$ candidate and Monte Carlo generated signal events; the horizontal lines demark the 3σ mass region* [14]. *Bottom right: as above with coordinates exchanged for $K_{e\mu\pi}$ candidate events; the box indicates the signal region. Bottom left: invariant mass distribution for $K_{\mu\mu\pi}$ candidate events; the dashed line indicates the expected signal* [17].

out to second order in the expansion in powers of the quark masses, and the uncertainties from higher order effects are estimated reliably for the first time. The resulting predictions $a_0^0 = 0.220 \pm 0.005$, and $a_0^2 = -0.0444 \pm 0.0010$ are in remarkable agreement with our new experimental result, which we will discuss in the following.

Figure 3 shows these predictions and also a number of older, alternative model theoretical predictions [25]. Since the extraction of the $\pi\pi$ amplitude in the high statistics $\pi N \to \pi\pi N$ experiments is model dependent, and the $\pi\pi$ atom data from the DIRAC experiment [26] are not yet available, one had to rely primarily on the K_{e4} data for the comparison between theory and experiment, which were not sufficiently accurate to discriminate between the different models.

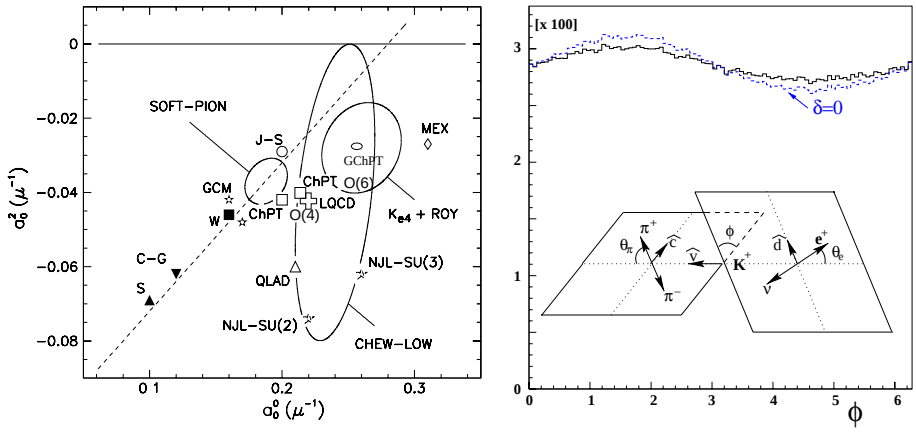

Figure 3: *Left: previous measurements and predictions* [25] *for the scattering length (taken from Ref.* [28]*). Right: azimuthal asymmetry averaged over all other kinematical quantities with standard phase $\pi\pi$ shifts and with phase shifts set to zero. Insert: kinematical quantities used in the description of K_{e4} decay.*

K_{e4} events are selected with a vertex within the decay tank of acceptable quality, a momentum reconstructed from the three daughter particles below the beam momentum. The momentum vector of the incoming K^+ is obtained from the hit in the pixel counter (see Fig. 1) and the vertex, and requiring the K^+ to come from the production target 27.5 m upstream as well as an unambiguous identification of the e^+ and the π^- in both Čerenkov counters

and the calorimeter. The event sample contains a small amount of background events, mainly from K_τ decay (1.3 ± 0.3 %) and accidentals (2.6 ± 0.2 %). A K_τ can fake a K_{e4} by either a misidentification of one of the π^+ due to δ-rays, photomuliplier noise or the presence of an additional positron, or a decay of one π^+ directly or via a μ^+ into a e^+. The dominating accidental background is a combination of a $\pi^+\pi^-$ pair from K_τ decay with a positron from either the beam or from a K_{dal} decay.

After event selection 406'103 events remain, of which we estimate 388270 $\pm$ 5025 to be K_{e4} events. This corresponds to an increase in statistics by more than a factor 12 compared with previous experiments [20].

Quantitative understanding and analysis of the data relies strongly on the quality of Monte Carlo simulation of the detector response. This GEANT-based [13] simulation is supplemented with separately measured efficiencies of the various detector parts, and was extensively tested against data in the various decay channel under study. Figure 4 shows a few control plots demonstrating the good agreement between measured and simulated distributions of the kinematic variables. The total Monte Carlo data sample comprises $81.6 \cdot 10^6$ generated K_{e4} events of which $2.9 \cdot 10^6$ were accepted after reconstruction and passage through the same analysis codes as the data. We also compare Monte Carlo with data distributions for the kinematically very distinct K_τ and K_{dal} decays, and are able to reproduce the measured branching ratios for these decays. A chiral perturbation theory calculation on the one loop level [27, 29, 30] is used to model the physics of the decay at this point. Radiative corrections are included following Diamant [31].

For the description of the K_{e4} decay three reference frames are commonly used (see Fig. 3): the K^+ rest system (Σ_K), the $\pi^+\pi^-$ rest system ($\Sigma_{\pi\pi}$) and the $e^+\nu$ rest system ($\Sigma_{e\nu}$). The decay kinematic is then fully described by five variables: $s_\pi = M^2_{\pi\pi}$, the invariant mass squared of the dipion; $s_e = M^2_{e\nu}$, the invariant mass squared of the dilepton; θ_π, the angle of the π^+ in $\Sigma_{\pi\pi}$ with respect to the direction of flight of the dipion in Σ_K; θ_e, the angle of the e^+ in $\Sigma_{e\nu}$ with respect to the direction of flight of the dilepton in Σ_K; ϕ, the angle between the plane formed by the pions in $\Sigma_{\pi\pi}$ and the corresponding plane formed by the leptons. The experimental resolution for these five variables is $\sigma(s_\pi) = 0.00133$ GeV^2, $\sigma(s_e) = 0.00361$ GeV^2, $\sigma(\theta_\pi) = 0.147$, $\sigma(\theta_e) = 0.111$ and $\sigma(\phi) = 0.404$.

The K_{e4} branching ratio is determined relative to K_τ decay ($\mathrm{Br}(\tau) = 5.59 \pm 0.05$ %), for which events were collected with a minmum bias trigger concurrently with K_{e4} events. We obtain

$$\mathrm{BR}(K_{e4}) = (4.109 \ \pm \ 0.008\ (\mathrm{stat.}) \pm 0.110\ (\mathrm{syst.})) \cdot 10^{-5}$$

The result is in agreement with the average of previous measurements: $(3.91 \pm 0.17) \cdot 10^{-5}$ [18]. The largest of the 17 contributions to the systematic error (2.68%), which we have evaluated, stem from the background subtraction (1.2%), the Čerenkov efficiencies (1.5%) and the K_τ branching ratio (0.9%).

The analysis of the K_{e4} decay distributions is far from trivial, and requires a fair amount of theoretical input. We list below the basic ingredients and prepare the notation for the subsequent result section.

The most general form of the decay matrixelement is written most conveniently using the following combinations of four-momenta and Lorentz invariants:

$$\begin{aligned} P = p_1 + p_2,\ Q = p_1 - p_2,\ L = p_e + p_\nu,\ X = [(P\cdot L)^2 - s_\pi s_e]^{1/2}\ , \\ M = \frac{G_F}{\sqrt{2}} V_{us}^* \overline{u}(p_\nu)\gamma_\mu(1-\gamma_5)v(p_e)(V^\mu - A^\mu)\ , \\ A^\mu = \frac{1}{M_K}\left(FP^\mu + GQ^\mu + RL^\mu\right)\ , \qquad V^\mu = \frac{H}{M_K^3}\epsilon^{\mu\nu\rho\sigma}L_\nu P_\rho Q_\sigma\ . \end{aligned} \tag{1}$$

F, G, R, H dimensionless complex functions of $p_1\cdot p_2$, $p_1\cdot p$, $p_2\cdot p$, or of s_π, s_e and θ_π. If terms $\propto M_e^2/s_e$ are neglected R does not contribute to the decay rate, first evaluated by Pais and Treiman [32]:

$$d\Gamma_5 = \frac{G_F^2 V_{us}^2}{2^{12}\pi^6 M_k^5} X \frac{2M_\pi q}{\sqrt{s_\pi}} J_5(s_\pi, s_e, \theta_\pi, \theta_e, \phi) ds_\pi ds_e d\cos\theta_\pi d\cos\theta_e d\phi\ . \tag{2}$$

For the detailed decomposition of the factor J_5 in the above expression in terms of the kinematical variables we must refer to Ref. [32, 33]. A convenient partial wave expansion of the form factors in the variable θ_π gives the following [33]:

$$\begin{aligned} F &= \left(f_s + f_s'\,q^2 + f_s''\,q^4 + f_e\,s_e\right)\exp(i\delta_0^0(s_\pi)) \\ &\qquad + \tilde{f}_p\,(q^2/s_\pi)^{1/2}\,(P\cdot L)\,\cos\theta_\pi\,\exp(i\delta_1^1(s_\pi))\ , \\ G &= \left(g_p + g_p'\,q^2 + g_e\,s_e\right)\exp(i\delta_1^1(s_\pi))\ , \\ H &= \left(h_p + h_p'\,q^2\right)\exp(i\delta_1^1(s_\pi))\ , \end{aligned} \tag{3}$$

where q is the pion momentum in $\Sigma_{\pi\pi}$, divided by M_π. This parameterization yields ten new form factors f_s, f_s', f_s'', f_e, $\tilde{f}_p$, g_p, g_p', g_e, h_p, and h_p', which do

not depend on any kinematical variables, plus the phases δ_0^0 and δ_1^1, which are still functions of s_π.

It is worth noting at this point, that the phase shifts enter into the decay rate only through interference terms, which are proportional to $\sin\phi$ or $\cos\phi$. The azimuthal ϕ asymmetry, which has an amplitude of only approximately 10% of the the average (Fig. 4), is principal source of the phase shift information as illustrated in Fig. 3.

There exist three slightly different possibilities to extract the form factor and phase shift information from the data. Firstly, we can use the parameterization given above in Eq. 3 and perform individual fits in bins of s_π respecting the s_π dependence of the phase shifts. Secondly, there is the option to express the phase shifts by Eq. 4 shown below. This allows to use the whole data sample in one single fit. Finally, we can employ in addition Eq. 5, reducing the number of parameters by one.

The phase shifts δ_0^0 and δ_1^1 can be related to the s-wave scattering lengths a_0^0 and a_0^2 by means of the Roy equations [34]. A recent analysis of the phase shift data [35] used the parametrisation proposed by Schenk [36]:

$$\tan\delta_\ell^I = \sqrt{1-\frac{4M_\pi^2}{s_\pi}}\; q^{2\ell}\left\{A_\ell^I + B_\ell^I q^2 + C_\ell^I q^4 + D_\ell^I q^6\right\}\left(\frac{4M_\pi^2 - s_\ell^I}{s_\pi - s_\ell^I}\right) \ . \qquad (4)$$

The Roy equations were solved numerically, expressing the parameters A_ℓ^I, B_ℓ^I, C_ℓ^I, D_ℓ^I, and s_ℓ^I as a function of the scattering lengths a_0^0 and a_0^2. The possible values of the scattering lenghts were restricted to a band in the $a_0^0 - a_0^2$ plane, the *universal band* introduced by Morgan and Shaw [37]. The centroid of this band, the *universal curve* can be expressed by a second degree polynominal, relating a_0^0 and a_0^2:

$$a_0^2 = -0.0849 + 0.232\, a_0^0 - 0.0865\, (a_0^0)^2 \qquad (5)$$

For the fits our data are divided over 6 bins in s_π, 5 bins in s_e, 10 bins in $\cos\theta_\pi$, 6 bins in $\cos\theta_e$, and 16 bins in ϕ, 28'800 bins in total with on average 13 events in each bin. In the χ^2 minimization procedure the number of measured events n_j in each bin j is compared to the number of expected events in that bin r_j given by

$$r_j = \frac{\mathrm{Br}(K_{e4})N(K^+)}{N(\text{Generated events})} \times \sum \frac{J_5(F^{New}(q), G^{New}(q), H^{New}(q))}{J_5(F^{MC}(q), G^{MC}(q), H^{MC}(q))} \ . \qquad (6)$$

F^{MC}, G^{MC}, and H^{MC} correspond to the original form factors used to generate the Monte Carlo event, while F^{New}, G^{New}, and H^{New} are the form factors derived from the parameters of the fit. q denotes the inital and not the reconstructed kinematical variables. Thus the parameters are applied on an event by event basis, and at the same time a possible bias caused by the initial choice of the matrix element is eliminated.

In a first step the form factors in each bin in s_π are fitted independently. It is further assumed that the form factors do not depend on s_e and that the form factor F contributes to s-waves only, i.e. $f_e = g_e = \tilde{f}_p = 0$ are fixed at zero. This leaves one parameter each to describe the form factors F, G, and H per bin plus the phase shift difference $\delta \equiv \delta_0^0 - \delta_1^1$. Figures 5 and 6 summarize the results for F, G and the phase shifts, respectively. The s_π dependence of F and G may be fitted with $f_s = 5.770 \pm 0.097$, $f_s' = 0.95 \pm 0.55$, $f_s'' = -0.52 \pm 0.58$ (quadratic fit) or with $f_s = 5.835 \pm 0.065$, $f_s' = 0.47 \pm 0.15$ (linear fit), and $g_p = 4.684 \pm 0.092$, $g_p' = 0.54 \pm 0.20$ (linear fit), respectively.

If the individual phase shifts are expressed in terms of the scattering length a_0^0 (Eq. 4), i.e. the *universal curve* is used to express a_0^2 as a function of a_0^0, and the form factors are parametrized as in Eq. 3, the results listed in Table 2 are obtained.

Table 2: *Results of the fits to the K_{e4} data using Eq. 3 and Eq. 5 ($\chi^2/NdF = 1.075$). For the last column the latter constraint is dropped. The other parameters and the χ^2 do not change significantly.*

f_s	$5.75 \pm 0.02 \pm 0.08$	g_p	$4.66 \pm 0.47 \pm 0.07$
f_s'	$1.06 \pm 0.10 \pm 0.40$	g_p'	$0.67 \pm 0.10 \pm 0.04$
f_s''	$-0.59 \pm 0.11 \pm 0.40$	h_p	$-2.95 \pm 0.19 \pm 0.20$
a_0^0	$0.228 \pm 0.012 \pm 0.003$	$\Rightarrow$ (UB) a_0^2	-0.036 ± 0.009
a_0^0	$0.203 \pm 0.033 \pm 0.004$	a_0^2	$-0.055 \pm 0.023 \pm 0.003$

In conclusion it can be stated, that the E865 results constitute a major advance in the program of precision tests of hadronic interaction models at low energies. They also do nicely confirm the updated two-loop ChPT predictions [10].

References

1. E865-Collaboration: D. Lazarus, H. Ma, P. Rehak (Brookhaven National Laboratory); G.S. Atoyan, VV. Issakov, A.A. Poblaguev (INR, Moscow); J. Egger, W.D. Herold, H. Kaspar (Paul Scherrer Institut); B. Bassalleck, S. Eilerts, H. Fischer, J. Lowe (New Mexico); R. Appel, D.N. Brown, N. Cheung, C. Felder, M. Gach, D.E. Kraus, P. Lichard, Alexandre Sher, J.A. Thompson (Pittsburgh); D. Bergman, S. Dhawan, H. Do, J. Lozano, W. Majid, M. Zeller (Yale); S. Pislak, Aleksey Sher, P. Truöl (Zürich).
2. M.L. Brooks *et al.*, Phys. Rev. Lett. **83** (1999), 1521.
3. J. Kaulard *et al.*, Phys. Lett. **B422** (1993), 334.
4. T. Mori *et al.*, PSI-Proposal R99-05 ($\mu^+ \to e^+\gamma$, 1999); W. Molzon *et al.*, MECO-Proposal at BNL ($\mu^- A \to e^- A'$, 2000); R. Engfer et al., PSI Proposal R87-03 ($\mu^- A \to e^- A'$).
5. see e.g. M. Nakahata, Super-Kamiokande coll., Nucl. Phys. Proc. Suppl. **87** (2000), 125.
6. D. Ambrose *et al.* Phys. Rev. Lett. **81** (1998), 5437.
7. A.M. Lee *et al.* Phys. Rev. Lett. **64** (1990), 165.
8. G.S. Atoyan *et al.*, Nucl. Instr. Meth. **A320** (1992), 144.
9. J. Gasser, and H. Leutwyler, Phys. Lett. **125B** (1983), 325.
10. G. Colangelo, J. Gasser, and H. Leutwyler, Phys. Lett. **B488** (2000), 261.
11. R. Appel *et al.*, Phys. Rev. Lett. **83** (1999), 4482.
12. H. Ma *et al.*, Phys. Rev. Lett. **84** (2000), 2580.
13. S. Pislak, Thesis, University of Zürich (1997). D. Bergman, Thesis, Yale University (1997).
14. R. Appel *et al.*, Phys. Rev. Lett. **85** (2000), 2450.
15. R.N. Cahn, and H. Harari, Nucl. Phys. **B176** (1980), 135.
16. O. Shanker, Nucl. Phys. **B85** (1981), 382.
17. R. Appel *et al.*, Phys. Rev. Lett. **85** (2000), 2877.
18. C. Caso *et al.*, Eur. Phys. J. **C15** (2000), 1.
19. L. Littenberg, and R. Shrock, Phys. Lett. **B491** (2000), 285.
20. L. Rosselet *et al.*, Phys. Rev. **D15** (1977), 574.
21. S. Weinberg, Phys. Rev. Lett. **17** (1966), 616.
22. G. Colangelo, in *Frascati 1999: Physics and detectors for DAPHNE*, p. 425-438; hep-ph/0001256

23. J. Bijnens *et al.*, Phys. Lett. **B374** (1996), 210.
24. J. Bijnens *et al.*, Nucl. Phys. **B508** (1997), 263; err. ibid. **B517** (1998), 639.
25. *GChPT*: M. Knecht *et al.*, Nucl. Phys. **B471** (1996), 445; *JS*: R.D Jacob, and M.D. Scadron, Phys. Rev. **D25** (1982), 3073; *QLAD*: A.N. Ivanov, and N.I. Troitskaya, Sov. J. Nucl. Phys. **43** (1986), 260; *MEX*: D. Lohse *et al.*, Nucl. Phys. **A516** (1990), 513; *NJL-SU(2)*: M.C. Ruivo *et al.*, Nucl. Phys. **A575** (1994), 460; *GCM*: C.D. Roberts *et al.*, Phys. Rev. **D49** (1994), 125; *LQCD*: Y. Kuramashi *et al.*, Phys. Rev. Lett. **71** (1993), 2387.
26. J. Schacher (DIRAC coll.), 3^{rd} Workshop on Chiral Dynamics - Chiral Dynamics 2000: Theory and Experiment, Newport News (July 2000), preprint hep-ph/0010085.
27. J. Bijnens, Nucl. Phys. **B337** (1990), 635.
28. D. Pocanic, in *Chiral Dynamics Workshop*, Cambridge, MA (1994), p. 95.
29. J. Bijnens, G. Ecker and J. Gasser, in DAPHNE Physics Handbook **1**, L. Maiani ed. (Frascati INFN - LNF-92-047, 1992), p. 115.
30. C. Riggenbach *et al.*, Phys. Rev. **D43** (1991), 127.
31. A.M. Diamant-Berger, Thesis, Centre d'Etudes Nucléaires de Saclay (1976), Report CEA-N-1918.
32. A. Pais, and S.B. Treiman, Phys. Rev. **168** (1967), 1858.
33. G. Amorós, and J. Bijnens, J. Phys. **G25** (1999), 1607.
34. S.M. Roy, Phys. Lett. **B36** (1971), 353.
35. B. Ananthanarayan *et al.*, preprint hep-ph/0005297.
36. A. Schenk, Nucl. Phys. **B363** (1991), 97.
37. D. Morgan, and G. Shaw, Nucl. Phys. **B10** (1969), 261.

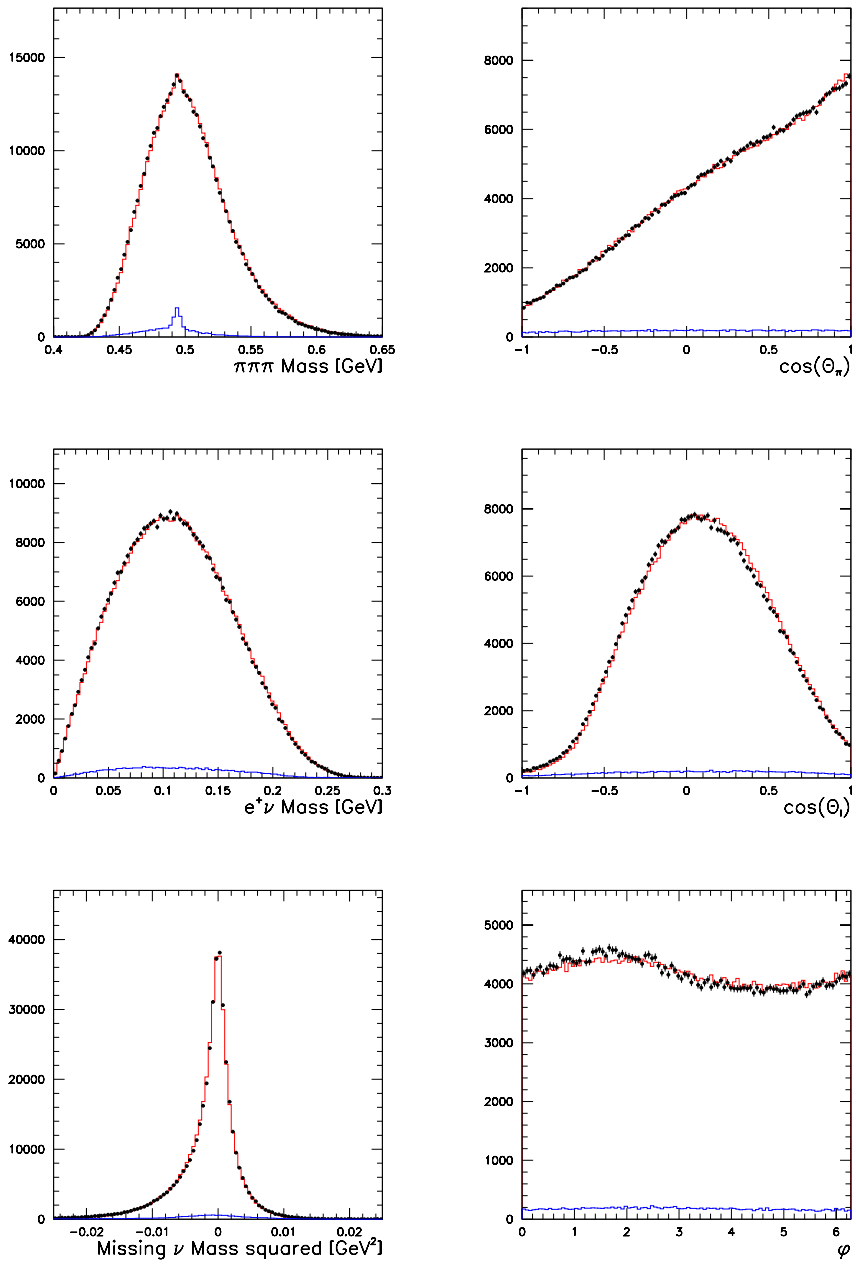

Figure 4: *K_{e4} control plots. From top left to bottom right: $\pi\pi$ mass; $\cos\theta_\pi$; $e\nu$ mass; $\cos\theta_e$; missing ν mass squared; ϕ. Data (solid circles), Monte Carlo (histogram) including backgrund, and background separately (lower histogram).*

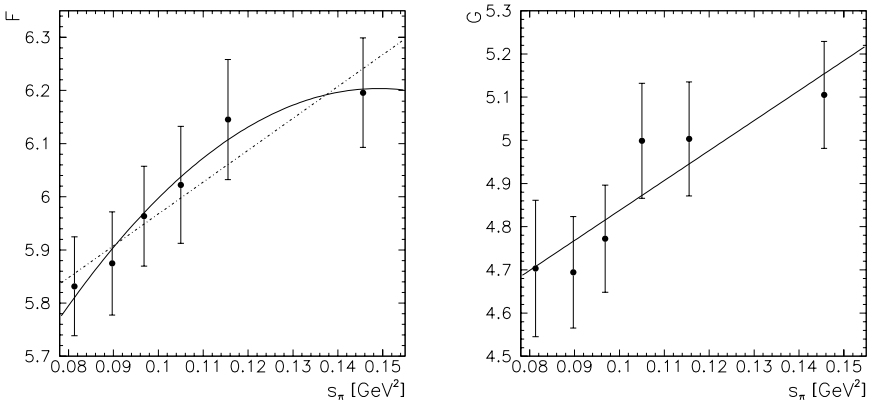

Figure 5: *Form factors F and G as function of s_π.*

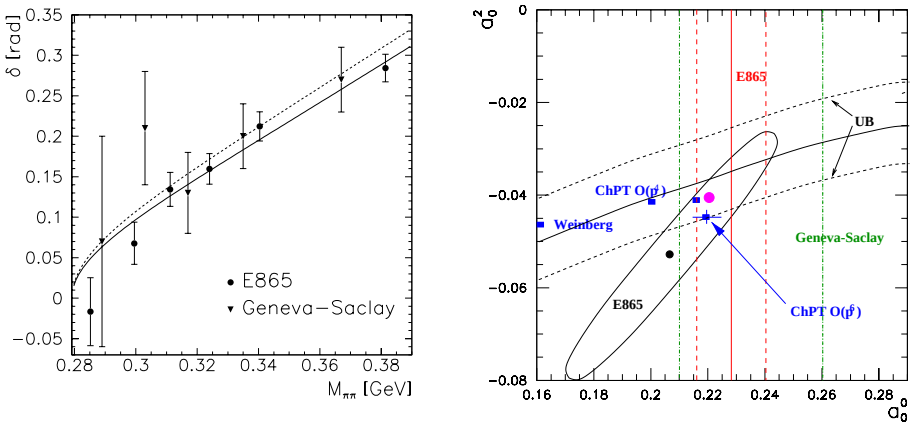

Figure 6: *Left: E865 phase shift results compared to the Geneva-Saclay data* [20]. *The lower curve is the result of the fit to our data. Right: $\pi\pi$ scattering length. The solid vertical line and the ellipse indicate our results for the scattering lengths for the two analyses requiring the universal curve (UB) as additional input or not. The solid squares indicate sucessive orders in chiral perturbation theory calculations, the latest of which* [10] *is marked with a cross. The solid circle indicates LQCD-result* [25]. *The dot-dashed lines indicate the center and lower error band of the previous experiment* [20].